ELSEVIER

Applied Numerical Mathematics 26 (1998) 435–464

APPLIED NUMERICAL MATHEMATICS

Modelling of compressible flows with highly oscillating initial data by homogenization ☆

Tomás Chacón Rebollo [a], Daniel Franco Coronil [a], Francisco Ortegón Gallego [a,*], Isabel Sánchez Muñoz [b]

[a] *Departamento de Ecuaciones Diferenciales y Análisis Numérico, Universidad de Sevilla, C/. Tarfia, s/n., 41080 Sevilla, Spain*

[b] *Departamento de Matemática Aplicada I, Universidad de Sevilla, C/. Tarfia, s/n., 41080 Sevilla, Spain*

Abstract

We introduce a mathematical modelling of slightly compressible viscous flows with two well-separated space scales. We use as mean tool formal mathematical homogenization techniques. In the model derived, there appear closure terms, much as in usual physical turbulence models. Here, the closure terms are computed from the solution of a PDE system that governs the turbulent perturbation. This system is coupled to the mean flow PDE system. Starting from this model, we derive another of the k–ε family, including eddy diffusion terms. We solve this model by an explicit mixed finite volume–finite element technique with upwinding. We test it for a compressible steady mixing layer with different convective Mach numbers. The numerical results show a good qualitative prediction of the relevant mean quantities of the flow for moderately high convective Mach numbers. This is consistent with the theoretical foundations of the model. © 1998 IMACS/Elsevier Science B.V.

Keywords: Reynolds stress modelling; Homogenization; k–ε model; Upwinding; Finite volumes; Finite elements

1. Introduction

During the last years many authors have applied homogenization techniques in Fluid Mechanics in order to study the evolution of certain kinds of turbulent flows. In [9] McLaughlin, Papanicolaou and Pironneau (MPP) applied these techniques to the Euler equation for ideal incompressible fluid flows with rapidly oscillating initial data; later on, the same ideas were extended to the Navier–Stokes equations for Newtonian incompressible and slightly viscous fluid flows [3,10,12].

☆ Research partially supported by DGICYT grant PB93-1196 and EU ETMA Brite-Euram Project.

* Corresponding author. Present address: Departamento de Matematicas, Universidad de Cadiz, C.A.S.E.M., Campus del Rio San Pedro, 11510 Puerto Real (Cadiz), Spain. E-mail: francisco.ortegon@uca.es.

PII S0168-9274(97)00069-X

Essentially, the MPP model of turbulence makes two basic assumptions. At first, it is assumed that the two length scales developed by the mean flow (L) and by the fluctuating field (l) are well separated; this is a length scale separation hypothesis. These two length scales allow us to define a dimensionless parameter $\delta = l/L$. Next, the model assumes that the initial velocity field is highly oscillating.

MPP modelling of incompressible flows uses formal mathematical homogenization techniques to derive averaged equations, intended to govern the mean quantities of the flows considered. Such techniques provide not only averaged equations, but also a microscale set of partial differential equations, that govern the universal (in some specific sense) behaviour of the fluctuating field. There are specific interaction terms in both averaged and microscale equations sets, that make them to be essentially coupled. In particular, in the averaged equations, there appear "closure" terms, that represent the averaged action of the fluctuating field on the mean flow.

MPP modelling is fully based upon formal mathematical arguments. MPP models differ remarkably from the usual turbulence models. In these latter, the averaging technique uses more heuristic mathematical arguments. Also, the "modelling" of closure terms is essentially based upon physical arguments [13].

Extensive numerical simulations have been done in order to validate the MPP modelling technique for incompressible flows. From the physical point of view, the main innovation of such modelling is that the Reynolds stress tensor here seems to model purely transient oscillatory effects, instead of turbulent diffusion. Concretely, this behaviour was observed in numerical simulations of three-dimensional homogeneous turbulence for wall-bounded flow [3,4]. Also, a comparison between a k–ε transient model and an MPP model including k but not h was made by Bègue et al. in [2] for two-dimensional flow past a cylinder. This experiment indicates that the production terms in the MPP model are relevant in regions where strong transient effects take place. The k–ε model fails to simulate appropriately these effects, although it is much more appropriate to model eddy diffusion effects.

Our purpose here is to derive an MPP model for compressible flows with two space scales, by taking advantage of the know-how acquired with incompressible flows. We shall also give some numerical tests that show the agreement of our model with the k–ε one for steady compressible mixing layer flow.

Our paper is organized as follows. In Section 2 we use homogenization techniques to derive an MPP model for inviscid perfect flows with two space scales. This is applied in Section 3 to obtain a transient model of the k–ε family, by adapting the techniques developed for incompressible flows. Section 4 is devoted to analyze the structure of closure terms appearing in the model. We use frame invariance to simplify their structure, and derive a model for 2D mean flows including theoretically smooth closure terms. In Section 5 we develop a strategy and a numerical technique for the computation of closure terms, as functions of certain parameters appearing in the model. We also give asymptotic behaviour of the closure terms for large values of these parameters. In Section 6 we perform a change of variables in the model in order to retrieve the law of state of perfect gases. This allows to adapt laminar solvers for Euler equations to the numerical solution of our model. Section 7 describes a numerical discretization of the model for unstructured triangular grids. Space discretization consist of a Galerkin technique that combines finite volume discretization for convection terms, with finite element discretization for diffusion and production terms. Van Leer's MUSCL method is used to compute the convective fluxes. For time discretization we use an explicit second-order four-stage Runge–Kutta method. A local time step strategy is used to perform an efficient computation of steady flows. Finally, in Section 8 we show some numerical results for steady compressible mixing layers. Our results show that our model agrees

closely with the k–ε one for such a kind of flows. This is consistent with the initial mathematical hypothesis of our model.

2. Homogenization of flows of inviscid perfect fluids

In this section we shall adapt the asymptotic techniques introduced in [9] to derive averaged equations for inviscid perfect fluids. These techniques were systematized in [4], where the physical and mathematical consistency of the model for incompressible flows was analyzed. Here, we shall apply the systematic technique of [4] to inviscid perfect fluids. Thus, we shall omit the intermediate calculations. We shall assume that density, velocity and internal energy (denoted, respectively, by ρ^δ, u^δ and e^δ) verify

$$\begin{cases} \rho^\delta_{,t} + \nabla\cdot(\rho^\delta u^\delta) = 0, \\ \rho^\delta\big(u^\delta_{,t} + (u^\delta\cdot\nabla)u^\delta\big) + (\gamma-1)\nabla(\rho^\delta e^\delta) = 0, \\ e^\delta_{,t} + u^\delta\nabla e^\delta + (\gamma-1)e^\delta\nabla\cdot u^\delta = 0, \end{cases} \tag{1}$$

where the constant γ stands for the specific heats ratio. Together with (1), we assume the highly oscillating initial conditions

$$\begin{cases} \rho^\delta(x,0) = \bar\rho_0(x) + \delta^{2/3}\rho_0\left(\dfrac{x}{\delta};x\right), \\ u^\delta(x,0) = \bar u_0(x) + \delta^{1/3}w_0\left(\dfrac{x}{\delta};x\right), \\ e^\delta(x,0) = \bar e_0(x) + \delta^{2/3}e_0\left(\dfrac{x}{\delta};x\right), \end{cases} \tag{2}$$

where $\rho_0(y;x)$, $w_0(y;x)$ and $e_0(y;x)$ are smooth functions, y-periodic in the cube $Y=[0,2\pi]^3$ and with zero mean. These are initial conditions with two space scales.

In order to study the behaviour of $(\rho^\delta,u^\delta,e^\delta)$ when $\delta\to 0$, we associate the following asymptotic expansions:

$$\begin{cases} \rho^\delta(x,t) = \bar\rho(x,t) + \delta^{1/3}\rho^{(0)}\left(\dfrac{a(x,t)}{\delta},\dfrac{t}{\delta^{2/3}};x,t\right) \\ \qquad + \delta^{2/3}\rho^{(1)}\left(\dfrac{a(x,t)}{\delta},\dfrac{t}{\delta^{2/3}};x,t\right) + \delta\rho^{(2)}\left(\dfrac{a(x,t)}{\delta},\dfrac{t}{\delta^{2/3}};x,t\right)+\cdots, \\ u^\delta(x,t) = \bar u(x,t) + \delta^{1/3}w\left(\dfrac{a(x,t)}{\delta},\dfrac{t}{\delta^{2/3}};x,t\right) \\ \qquad + \delta^{2/3}u^{(1)}\left(\dfrac{a(x,t)}{\delta},\dfrac{t}{\delta^{2/3}};x,t\right) + \delta u^{(2)}\left(\dfrac{a(x,t)}{\delta},\dfrac{t}{\delta^{2/3}};x,t\right)+\cdots, \\ e^\delta(x,t) = \bar e(x,t) + \delta^{1/3}e^{(0)}\left(\dfrac{a(x,t)}{\delta},\dfrac{t}{\delta^{2/3}};x,t\right) \\ \qquad + \delta^{2/3}e^{(1)}\left(\dfrac{a(x,t)}{\delta},\dfrac{t}{\delta^{2/3}};x,t\right) + \delta e^{(2)}\left(\dfrac{a(x,t)}{\delta},\dfrac{t}{\delta^{2/3}};x,t\right)+\cdots. \end{cases} \tag{3}$$

Here $\rho^{(0)}(y,\tau;x,t)$, ..., $w(y,\tau;x,t)$, $u^{(1)}(y,\tau;x,t)$, ..., $e^{(0)}(y,\tau;x,t)$, ... are assumed to be smooth functions, y-periodic in Y and bounded in τ.

Also, $a(x,t)$ are the inverse Lagrangian coordinates related to the mean velocity field $\bar{u}$,

$$\begin{cases} a_{,t} + (\bar{u}\cdot\nabla)a = 0, \\ a(x,0) = 0. \end{cases} \tag{4}$$

Following the techniques introduced in [9], we deduce at first that such an expansion can hold only if $\rho^{(0)}$ and $e^{(0)}$ are zero. Also, the perturbation w is determined through the solution $\widetilde{w}$ of a "canonical microstructure problem". This problem governs the microscale behaviour of the main turbulent perturbation. If w_0 is assumed to be odd in y and periodic, $\delta^{1/3}w$ is given by $\delta^{1/3}w = \sqrt{k}\,G^{-\mathrm{T}}\widetilde{w}$. ($A^{\mathrm{T}}$ states for the transpose of A and $G^{-\mathrm{T}}$ denotes the transpose of the matrix G^{-1}.)

$$\begin{cases} \widetilde{w}_{,\tau} + (\widetilde{w}\cdot\nabla_y)\widetilde{w} + C\nabla_y\pi = 0, \qquad \nabla_y\cdot\widetilde{w} = 0 \quad \text{in } \mathbb{R}^3\times\mathbb{R}, \\ \widetilde{w}(y,0) = \widetilde{w}_0(y) = \dfrac{1}{\sqrt{q_0}}w_0(y), \qquad q_0 = \dfrac{1}{2}\langle w_0^* C^{-1} w_0\rangle \quad \text{in } \mathbb{R}^3, \\ \widetilde{w},\pi \quad y\text{-periodic in } \mathbb{R}^3, \text{ bounded in } \tau;\ \widetilde{w} \text{ odd}, \end{cases} \tag{5}$$

where C is the symmetric matrix given by

$$C = G^*G, \qquad G = \nabla a \quad \left(G_{ij} = \frac{\partial a_j}{\partial x_i}\right)$$

and $\langle\cdot\rangle$ denotes the y-average on a period cell, $\langle v\rangle = (1/|Y|)\int_Y v$.

System (5) presents some conservation properties: The mean and mean kinetic energy of $\widetilde{w}$ are conserved in time τ. This can happen only if the averaged values of the terms appearing in the expansions (3) verify certain compatibility conditions [4]. Up to the second order, these equations are the following:

$$\begin{cases} \left[\begin{array}{l} \bar{\rho}_{,t} + \nabla\cdot(\bar{\rho}\bar{u}) = 0, \\ \bar{\rho}\big(\bar{u}_{,t} + (\bar{u}\cdot\nabla)\bar{u}\big) + (\gamma-1)\nabla(\bar{\rho}\bar{e}) = 0, \\ \bar{e}_{,t} + \bar{u}\nabla\bar{e} + (\gamma-1)\bar{e}\nabla\cdot\bar{u} = 0, \end{array}\right. \\ \left[\begin{array}{l} \bar{\rho}^{(1)}_{,t} + \nabla\cdot\big(\bar{\rho}^{(1)}\bar{u}\big) + \nabla\cdot\big(\bar{\rho}\bar{u}^{(1)}\big) = 0, \\ \bar{\rho}\big(\bar{u}^{(1)}_{,t} + (\bar{u}\cdot\nabla)\bar{u}^{(1)} + \big(\bar{u}^{(1)}\cdot\nabla\big)\bar{u}\big) + (\gamma-1)\nabla\cdot\big(\bar{\rho}\bar{e}^{(1)} + \bar{e}\bar{\rho}^{(1)}\big) \\ \quad + \bar{\rho}^{(1)}\big(\bar{u}_{,t} + (\bar{u}\cdot\nabla)\bar{u}\big) + \nabla\cdot(\bar{\rho}R) = 0, \\ \bar{e}^{(1)}_{,t} + \bar{u}\nabla\bar{e}^{(1)} + (\gamma-1)\bar{e}^{(1)}\nabla\cdot\bar{u} + \bar{u}^{(1)}\nabla\bar{e} + (\gamma-1)\bar{e}\nabla\cdot\bar{u}^{(1)} = 0, \\ (\bar{\rho}k)_{,t} + \bar{u}\nabla(\bar{\rho}k) + \bar{\rho}\delta^{2/3}R : \nabla\bar{u} + (\bar{\rho}k)\nabla\cdot\bar{u} = 0. \end{array}\right. \end{cases} \tag{6}$$

If we denote by $\langle\langle\cdot\rangle\rangle$ the y–τ-average given by

$$\langle\langle v\rangle\rangle = \lim_{\theta\to\infty}\frac{1}{\theta}\int_0^\theta \langle v\rangle \,\mathrm{d}\tau,$$

then the Reynolds stress tensor (RST) above is formally given by

$$R = \langle\langle w\otimes w\rangle\rangle, \tag{7}$$

whereas $k = \frac{1}{2}\delta^{2/3}\langle|w|^2\rangle$ is the mean kinetic turbulent energy.

Note that the fluctuation $\widetilde{w}$ is incompressible in the y-variable. As a consequence, we can only expect our model to be valid when the effects of the compressibility of the perturbation are not relevant. Note that this is also assumed in the usual derivation of turbulence models for compressible flows at moderate Mach numbers: the density fluctuations are neglected [15,18].

The microscale behaviour of turbulence found here is the same found when modelling turbulent incompressible flows by homogenization [4,9].

Note that the first terms in expansion (3) satisfy the original equations of perfect fluids. The effects of the perturbation are present in the equations for $(\bar\rho^{(1)},\bar u,\bar e^{(1)})$ by means of the tensor R. However, no "eddy viscosity" is present here. In fact, the energy $E^\delta = \rho^\delta(e^\delta + |u^\delta|^2/2)$ admits an asymptotic expansion $E^\delta = \overline{E}+\delta^{1/3}E^{(1)}+\cdots$ derived from (3). From system (6), $\overline{E}$ and $\overline{E}^{(1)}$ verify the following conservation laws:

$$\begin{aligned}
&\overline{E}_{,t} + \nabla\cdot\big[\big(\overline{E}+\bar p\big)\bar u\big] = 0, \quad \bar p = (\gamma-1)\bar\rho\bar e,\\
&\overline{E}^{(1)}_{,t} + \nabla\cdot\big[\big(\overline{E}^{(1)}+\bar p^{(1)}\big)\bar u + \big(\overline{E}+\bar p\big)\bar u^{(1)}\big] + \nabla\cdot(\bar\rho R\bar u) = 0,\\
&\bar p^{(1)} = (\gamma-1)\big(\bar\rho^{(1)}\bar e + \bar\rho\bar e^{(1)}\big).
\end{aligned}$$

At this stage, we should stress the fact that the same set of equations for both $\overline{E}$ and $\overline{E}^{(1)}$ is obtained if we start from the conservative form of (1) and then apply the same averaging process. This proves the consistency of such a technique.

3. Modelling of Reynolds stress tensor

As we have stated in the preceding section, the above modelling of Reynolds stress tensor does not introduce eddy diffusion in our model. In the incompressible case it rather appears as modelling a transient oscillatory interaction between large and small structures [2]. However, homogenization techniques also provide eddy diffusion terms when modelling incompressible flows. In [3] it is shown that if we extend the averaging process to one more term of our asymptotic expansion, the RST is modelled as follows:

$$\overline{u'\otimes u'} \simeq \delta^{2/3}R(C) - \nu_{\mathrm{T}}\delta\sqrt{k}\big(\nabla\bar u + \nabla\bar u^*\big), \quad u' = \delta^{1/3}w + \delta^{2/3}u^{(1)} + \cdots, \tag{8}$$

where ν_{T} is a numerical coefficient of eddy viscosity. However, some numerical experiments reported in [2] make it apparent that the levels of numerical diffusion given by (8) are too low. In [2] a "mixed"

modelling is proposed: the transient effects are modelled by homogenization, and the eddy diffusion effects are modelled as in the k–ε model, by means of the Boussinesq's hypothesis:

$$\overline{u' \otimes u'} \simeq \delta^{2/3} R(C) - \mu_{\mathrm{T}}\big(\nabla \bar{u} + \nabla \bar{u}^*\big). \tag{9}$$

This kind of modelling has been tested in [2] with encouraging results.

Our purpose here is to adapt (9) to perfect flows. In the usual modelling of turbulence, when modelling the Reynolds stress tensor by Boussinesq's hypothesis, the Reynolds ($\bar{u}$) and Favre ($\widetilde{u} = \overline{\rho u}/\bar{\rho}$) average are identified. We shall here replace the Reynolds mean by the integral mean about the y-variable, and identify it to the Favre mean.

In the k–ε model [8,10] the Reynolds stress tensor is modelled by

$$\overline{\rho u' \otimes u'} \simeq \tfrac{2}{3}\bar{\rho} k I - \mu_{\mathrm{T}} \mathcal{T}(\bar{u}), \tag{10}$$

where $\mathcal{T}(\bar{u})$ denotes the stress tensor,

$$\mathcal{T}(\bar{u}) = \tfrac{2}{3}\nabla \cdot \bar{u}\, I - \big(\nabla \bar{u} + \nabla \bar{u}^*\big).$$

Also, μ_{T} is the eddy viscosity coefficient, given by

$$\mu_{\mathrm{T}} = C_\mu \frac{k^2}{\varepsilon}, \quad C_\mu = 0.09,$$

and ε is the rate of viscous dissipation.

Following the ideas of Bègue et al. for incompressible flows, we propose the modelling of the Reynolds stress tensor for compressible flows given below

$$\overline{\rho u' \otimes u'} \simeq R = \delta^{2/3} \rho \langle\!\langle w \otimes w \rangle\!\rangle - \mu_{\mathrm{T}} \mathcal{T}(\bar{u}) = \rho k G^{-\mathrm{T}} \langle\!\langle \widetilde{w} \otimes \widetilde{w} \rangle\!\rangle G^{-1} - \mu_{\mathrm{T}} \mathcal{T}(\bar{u}). \tag{11}$$

In the sequel, we shall drop the bars to indicate averaged quantities. If we put this modelling of RST into the k–ε model for viscous perfect fluids, we obtain the following system of averaged equations:

$$\begin{cases}
\dfrac{\partial \rho}{\partial t} + \nabla \cdot (\rho u) = 0, \\
\dfrac{\partial (\rho a)}{\partial t} + \nabla \cdot (\rho a \otimes u) = 0, \\
\dfrac{\partial (\rho u)}{\partial t} + \nabla \cdot [\rho u \otimes u + pI] - \nabla \cdot \big[\mu \mathcal{T}(u) - R\big] = 0, \\
\dfrac{\partial E}{\partial t} + \nabla \cdot \big[(E+p)u\big] + \nabla \cdot \big[\big(R - \mu \mathcal{T}(u)\big)u\big] \\
\quad -\nabla \cdot \left[\left(\dfrac{\gamma \mu}{\mathrm{Pr}} + \dfrac{\gamma \mu_{\mathrm{T}}}{\mathrm{Pr}_{\mathrm{T}}}\right)\nabla e\right] - \nabla \cdot \left(\dfrac{\mu_{\mathrm{T}}}{\sigma_k}\nabla k\right) = 0, \\
\dfrac{\partial (\rho k)}{\partial t} + \nabla \cdot (\rho k u) - \nabla \cdot \left[\left(\mu + \dfrac{\mu_{\mathrm{T}}}{\sigma_k}\right)\nabla k\right] - P + \rho \varepsilon = 0, \\
\dfrac{\partial (\rho \varepsilon)}{\partial t} + \nabla \cdot (\rho \varepsilon u) - \nabla \cdot \left[\left(\mu + \dfrac{\mu_{\mathrm{T}}}{\sigma_\varepsilon}\right)\nabla \varepsilon\right] - C_{\varepsilon 1}\dfrac{\varepsilon}{k} P + C_{\varepsilon 2} \rho \dfrac{\varepsilon^2}{k} = 0, \\
p = (\gamma - 1)\big(E - \tfrac{1}{2}\rho |u|^2 - \rho k\big),
\end{cases} \tag{12}$$

where $E = \rho e + \frac{1}{2}\rho|u|^2$ is the total energy, Pr and $\mathrm{Pr_T}$ are the Prandtl number and the turbulent Prandtl number, respectively; the constant γ is the same as in (1), and σ_k, σ_ε, $C_{\varepsilon 1}$ and $C_{\varepsilon 2}$ are numerical constants (in our experiments, we have taken $\mathrm{Pr} = 0.72$, $\sigma_k = 1$, $\sigma_\varepsilon = 1.3$, $C_{\varepsilon 1} = 1.44$ and $C_{\varepsilon 2} = 1.92$).

This new model has certainly a higher complexity than the standard k–ε model. Indeed, we have new closure terms that depend on the inverse Lagrangian coordinates $a(x,t)$. However, the equation satisfied by this field is just a pure transport and it may be very efficiently solved, as we shall see in Section 7. Also, the closure terms may be tabulated by solving the canonical microstructure problem (5), and given as data to system (12). In exchange to this, we obtain a model that may allow us to simulate some some specific transient effects of the interactions large–small structures, as in the incompressible case [3].

The production term in the k and ε equations is $P = -R : \nabla u$.

4. Closure terms for 2D mean flows

In this section we briefly describe the structure of closure terms for 2D mean flows. We shall use the frame invariance of the model equations in order to gain a large simplifications of the structure of closure terms. This is an adaptation of the technique developed at first for incompressible flows.

4.1. Structure of closure terms

If model (5) is frame-invariant, then the tensor

$$\widetilde{R} = \widetilde{R}(C) = \langle\!\langle w \otimes w \rangle\!\rangle,$$

must also be frame-invariant, in the sense that

$$\widetilde{R}\big(Q^* C Q\big) = Q^* \widetilde{R}(C) Q,$$

for any orthogonal matrix Q. This is the case if the initial perturbation w is in turn frame invariant, cf. [4]. Rivlin–Ericksen's theorem leads to the following structure for $\widetilde{R}$ [5]:

$$\widetilde{R}(C) = \widetilde{\alpha}_0 I + \widetilde{\alpha}_1 C + \widetilde{\alpha}_2 C^2,$$

where $\widetilde{\alpha}_0$, $\widetilde{\alpha}_1$ and $\widetilde{\alpha}_2$ are coefficients depending only on the three invariants of matrix C, namely

$$i_1 = \operatorname{trace} C, \qquad i_2 = \det C, \qquad i_3 = \operatorname{trace} \operatorname{Adj} C.$$

By Cayley–Hamilton's theorem, we then have

$$\langle\!\langle w \otimes w \rangle\!\rangle(G) = \langle\!\langle w \otimes w \rangle\!\rangle\big(\widehat{C}\big) = \alpha_0 I + \alpha_1 \widehat{C} + \alpha_2 \widehat{C}^2,$$

where

$$\widehat{C} = GG^*, \qquad \alpha_0 = \frac{i_3}{i_2}\widetilde{\alpha}_0 + \widetilde{\alpha}_1, \qquad \alpha_1 = \widetilde{\alpha}_2 - \frac{i_1}{i_2}\widetilde{\alpha}_0, \qquad \alpha_2 = \frac{1}{i_2}\widetilde{\alpha}_0.$$

In our case, we shall consider 2D mean flows of the form

$$u(x,t) = \big(u_1(x_1, x_2, t), u_2(x_1, x_2, t), 0\big)^*.$$

Then,

$$a(x,t) = \big(a_1(x_1,x_2,t), a_2(x_1,x_2,t), x_3\big)^*,$$

and

$$G = \nabla a = \left[\begin{array}{cc|c} & M & 0 \\ & & 0 \\ \hline 0 & 0 & 1 \end{array}\right], \qquad C = \left[\begin{array}{cc|c} & D & 0 \\ & & 0 \\ \hline 0 & 0 & 1 \end{array}\right], \qquad \widehat{C} = \left[\begin{array}{cc|c} & \widehat{D} & 0 \\ & & 0 \\ \hline 0 & 0 & 1 \end{array}\right],$$

where $D = M^*M$, $\widehat{D} = MM^*$.

As $\widehat{D}$ satisfies

$$\widehat{D}^2 - \big(\operatorname{trace}\widehat{D}\big)\widehat{D} + \big(\det\widehat{D}\big)I = 0,$$

we are led to the following structure for tensor $\langle\langle w \otimes w\rangle\rangle$:

$$\langle\langle w \otimes w\rangle\rangle = \left[\begin{array}{cc|c} & \beta_0 I + \beta_1 \widehat{D} & 0 \\ & & 0 \\ \hline 0 & 0 & \beta_2 \end{array}\right] \tag{13}$$

with

$$\beta_0 = \frac{i_1 - 1}{i_2}\widetilde{\alpha}_0 + \widetilde{\alpha}_1, \qquad \beta_1 = \widetilde{\alpha}_2 - \frac{1}{i_2}\widetilde{\alpha}_0, \qquad \beta_2 = \widetilde{\alpha}_0 + \widetilde{\alpha}_1 + \widetilde{\alpha}_2. \tag{14}$$

If we denote the two invariants of $\widehat{D}$ by

$$j_1 = \operatorname{trace}\widehat{D}, \qquad j_2 = \det\widehat{D},$$

then, we have

$$i_1 = j_1 + 1, \qquad i_2 = j_2, \qquad i_3 = j_1 + j_2.$$

This shows that β_0, β_1 and β_2 are functions of j_1 and j_2 only.

As a conclusion, in the case of 2D mean flow, we can replace the RST modelling in (11) by

$$\overline{\rho u' \otimes u'} \simeq R = \rho k \Phi\big(\widehat{D}(u)\big) - \mu_T \mathcal{T}(u), \tag{15}$$

where

$$\Phi\big(\widehat{D}\big) = \left[\begin{array}{cc|c} & \beta_0 I + \beta_1 \widehat{D} & 0 \\ & & 0 \\ \hline 0 & 0 & \beta_2 \end{array}\right].$$

4.2. Definition of smooth closure terms

The coefficients β_0 and β_1 are computed from tensor $\widetilde{R} = \langle\langle \widetilde{w} \otimes \widetilde{w} \rangle\rangle$ issued from the solution of (5). An analogous derivation to that above yields

$$\widetilde{R} = \left[\begin{array}{cc|c} & & 0 \\ & \widetilde{\beta}_0 I + \widetilde{\beta}_1 D & 0 \\ \hline 0 & 0 & \widetilde{\beta}_2 \end{array}\right], \tag{16}$$

where

$$\widetilde{\beta}_0 = \widetilde{\alpha}_0 - j_2\widetilde{\alpha}_2, \qquad \widetilde{\beta}_1 = \widetilde{\alpha}_1 + j_1\widetilde{\alpha}_2, \qquad \widetilde{\beta}_2 = \widetilde{\alpha}_0 + \widetilde{\alpha}_1 + \widetilde{\alpha}_2.$$

Using identities (14) and (16) we deduce

$$\mu_1 = \widetilde{R}_{11} + \widetilde{R}_{22} = 2\widetilde{\beta}_0 + j_1\widetilde{\beta}_1 = j_1\beta_0 + \left(j_1^2 - 2j_2\right)\beta_1, \tag{17}$$

$$\mu_2 = \widetilde{R}_{33} = \widetilde{\beta}_2 = \beta_2. \tag{18}$$

We also have from (15) that

$$2 = \operatorname{trace}\Phi\left(\widehat{D}\right) = 2\beta_0 + j_1\beta_1 + \beta_2. \tag{19}$$

Eqs. (17)–(19) represent a linear system to determine β_0, β_1 and β_2 in terms of μ_1 and μ_2. This will only be possible if its determinant Δ is not equal to zero. Δ is zero only if

$$j_1^2 = 4j_2. \tag{20}$$

This is the equation of the parabolic boundary of the region of the admissible j_1 and j_2, given in (25). In this case, matrix D in (16) is proportional to the identity. Then, system (17)–(19) has infinitely many solutions, as solving (17) and (18) in β_0 and β_2 yields also a solution of (19) for each given β_1. Thus, the coefficients β_0, β_1 and β_2 are not uniquely defined.

In order to solve this difficulty, we may express $\Phi(\widehat{D})$ in terms of an orthogonal base of the space of 2×2 matrices spanned by I and $\widehat{D}$. If such space has dimension two, this orthogonal base is $\{I, \widehat{B}\}$, where $\widehat{B} = \widehat{D} - \frac{1}{2}j_1 I$. When $\widehat{D}$ is proportional to the identity, this base is reduced to $\{I\}$. In any case, we may write $\Phi(\widehat{D})$ as

$$\Phi\left(\widehat{D}\right) = \kappa I + \beta_1\widehat{B}, \quad \text{where } \kappa = \beta_0 + \tfrac{1}{2}j_1\beta_1. \tag{21}$$

Notice that in particular trace $\widehat{B} = 0$, and that such a decomposition is unique.

From system (17)–(19) we obtain

$$\kappa = \tfrac{1}{2}(2 - \mu_2), \tag{22}$$

$$\beta_1 = \frac{2}{\Delta}(\mu_1 - j_1\kappa). \tag{23}$$

Now, if $\widehat{D}$ is proportional to the identity, (22) still holds and $\widehat{B} = 0$. Thus, the value of β_1 is irrelevant. This ensures that decomposition (21) is well defined. Moreover, if we assume that the transformation

$C \mapsto \widetilde{R}(C)$ is continuous, so does it for coefficient κ; as $\kappa = \kappa(C) = \frac{1}{2}[2 - \widetilde{R}_{33}]$. Thus, β_1 is also continuous at matrices $\widehat{D}$ such that $\lambda_1 \neq \lambda_2$.

Consider now a matrix $\widehat{D}_0$ proportional to the identity ($\lambda_1 = \lambda_2$). Then,

$$\Phi(\widehat{D}_0) = \kappa(\widehat{D}_0) I.$$

Given $\widehat{D}$ in neighbourhood of $\widehat{D}_0$ such that $\lambda_1(D) \neq \lambda_2(D)$, we have

$$\beta_1(\widehat{D})\widehat{B} = \Phi(\widehat{D}) - \kappa(\widehat{D})I = [\Phi(\widehat{D}) - \Phi(\widehat{D}_0)] + [\kappa(\widehat{D}_0) - \kappa(\widehat{D})]I.$$

Then,

$$\lim_{\widehat{D}\to\widehat{D}_0} \beta_1(\widehat{D})\widehat{B} = 0.$$

As a consequence, the two summands of the decomposition of $\Phi(\widehat{D})$ given by (21) are continuous functions of $\widehat{D}$, if $\widetilde{R}$ is itself continuous.

It is important to remark that in practice, the tabulated parameters μ_1 and μ_2 must be furnished to the numerical code as data. Then, κ and β_1 are computed by (22) and eventually (23) for each needed D. This ensures that the trace of tensor R in (11) is exactly preserved to $2\rho k$. Otherwise, some artificial pressure will be created in the interpolation of κ and β_1.

In the sequel we shall still write β_0 instead of κ in order to simplify the notation.

5. Computation of closure terms

In this section, we describe the numerical solution technique to the canonical microstructure problem (5), and its application to the computation of the closure terms in model (12).

Identities (13) and (14) state that the Reynolds tensor $\langle\langle w \otimes w \rangle\rangle$ issued from homogenization depends only on the two invariants j_1 and j_2 of matrix D. This suggests to compute β_0 and β_1 as functions of these invariants, for diagonal matrices. We also must compute $\partial\beta_0/\partial j_1$ and $\partial\beta_0/\partial j_2$, as these quantities appear as closure terms in the equations for the energy in (32) (see Section 6).

We thus consider the matrices

$$C = \left[\begin{array}{c|c} D & \\ \hline & 1 \end{array}\right], \quad \text{with } D = \begin{bmatrix} \lambda_1 & \\ & \lambda_2 \end{bmatrix}. \tag{24}$$

Notice that as C is symmetric, we must take only $\lambda_1, \lambda_2 \in \mathbb{R}$. As

$$j_1 = \lambda_1 + \lambda_2, \qquad j_2 = \lambda_1\lambda_2,$$

then λ_1 and λ_2 are the (real) solutions of

$$\lambda^2 - j_1\lambda + j_2 = 0.$$

Consequently, we must only consider j_1, j_2 such that the discriminant of this equation is non-negative,

$$\Delta = j_1^2 - 4j_2 \geqslant 0. \tag{25}$$

Notice also that we may restrict ourselves to $j_1 > 0$, $j_2 > 0$, because C is positive definite.

5.1. Least squares solution of the canonical microstructures problem

In order to compute our canonical tensor $\widetilde{R}$ we have solved the steady-state version of system (5) verified by the canonical fluctuation $\widetilde{w}$, following the technique developed by Chacón and Ortegón in [3,12]. The steady-state version of the canonical microstructures problem is given by

$$\begin{cases} (\widetilde{w}\cdot\nabla_y)\widetilde{w} + C\nabla_y\pi = 0, \qquad \nabla_y\cdot\widetilde{w} = 0 \quad \text{in } Y =]0,2\pi[^3, \\ (\widetilde{w},\pi) \text{ odd and } Y\text{-periodic}, \\ \frac{1}{2}\langle \widetilde{w}^* C^{-1}\widetilde{w}\rangle = 1, \qquad \langle\widetilde{w}\rangle = 0. \end{cases} \tag{26}$$

In [12] it is shown that this problem has infinitely many solutions. However, this system is invariant under rotations of the frame of reference that leave unchanged the cube Y. In order to isolate one solution, we will be interested in discrete solutions that verify these invariances.

The solution technique is based upon a least squares formulation of (26). To describe it, let us denote by $H_p^k(Y)$, $k \geqslant 0$, the subspace of $H^k_{\text{loc}}(\mathbb{R}^3)$ of periodic functions on $\mathbb{R}^3$ with period cell Y. Define the subspaces

$$V_0 = \big\{v \in \big(H_p^1(Y)\big)^3 \,\big|\, \nabla\cdot v = 0,\ \langle v\rangle = 0\big\}, \qquad L^2_{p,0} = \big\{q \in L_p^2(Y) \,\big|\, \langle q\rangle = 0\big\}.$$

We intend to obtain a solution $(\widetilde{w},\pi)$ of (26) in the space $V_0 \times L^2_{p,0}$.

For a given trial couple $(\widetilde{w},\pi) \in V_0 \times L^2_{p,0}(Y)$, we associate an "error" couple $(e,p) \in (H_p^1(Y))^3 \times L_p^2(Y)$ as the solution to the problem

$$\begin{aligned} -\nabla_y\cdot(C\nabla_y p) &= \nabla_y\cdot\big[(\widetilde{w}\cdot\nabla_y)\widetilde{w}\big] \quad \text{in } Y, \qquad \langle p\rangle = 0, \\ -\Delta_y e &= \nabla_y\cdot\big[\widetilde{w}\otimes\widetilde{w} + C\pi\big] \quad \text{in } Y, \qquad \langle e\rangle = 0. \end{aligned}$$

Denote by $q(\widetilde{w})$ the kinetic energy of $\widetilde{w}$, and define the function

$$v = \frac{\widetilde{w}}{q(\widetilde{w})}.$$

Then we define the functional error J as

$$J(\widetilde{w}) = \int_Y \big|\nabla e(v)\big|^2.$$

Observe that J measures the error made when approximating the solution of (26) by $\widetilde{w}$. The normalization by $q(\widetilde{w})$ is due to the fact that the error e is homogeneous of degree two. Then, J is homogeneous of degree zero.

We now look for the solution of (26) as solution of the optimization problem

$$\begin{cases} \text{To obtain } \widehat{w} \in V_0 \text{ such that} \\ \quad J(\widehat{w}) = \min\limits_{w\in V_0} J(w). \end{cases} \tag{27}$$

The equivalence between (26) and (27) may be proved under certain restrictions on $\widetilde{w}$ [12].

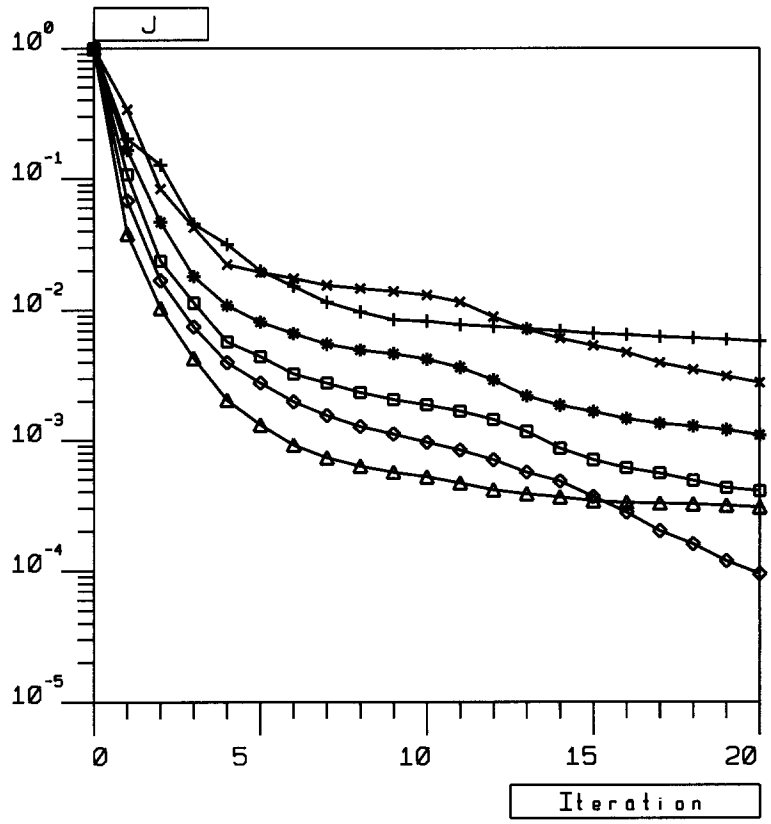

Fig. 1. Normalized cost J defined in Section 5.1, for $j_2 = 0.25$ and different values of j_1: 1.00 (+—+—+), 1.27 (✱—✱—✱), 1.54 (✱—✱—✱), 1.82 (□—□—□), 2.09 (◇—◇—◇) and 2.37 (△—△—△).

Problem (27) has been discretized by the finite element method, approximating $(\widetilde{w}, \pi)$ by the P_1-iso P_2 element on tetrahedra. Uniform $9 \times 9 \times 9$ and $17 \times 17 \times 17$ grids have been used to discretize velocities and pressures, respectively. Fast Fourier transform has been used to inverse the elliptic linear operators that appear in the equations for p and e above as well as to solve the corresponding adjoint problems.

Special care is taken to obtain discrete solutions that verify the invariances of the problem. In particular, it is especially important that if matrix C is diagonal, then the computed tensor $\widetilde{R}$ be also diagonal. This is obtained numerically up to a precision of 10^{-12}.

Also, the discrete optimization resulting problem has been solved by a conjugate gradient method, with projection on the set of functions with unit kinetic energy. In [12] a detailed description of this solution technique may be found.

This technique allows to compute approximate solutions to (26) that numerically appear as "locally unique": they are rather independent of the initializations of the conjugate gradient process if these vary in the neighbourhood of a given initialization.

Fig. 1 represents the evolution of the normalized cost J versus the iterations of the conjugate gradient process. In mean, the initial cost J is divided by 1000 in approximately 20 iterations. This

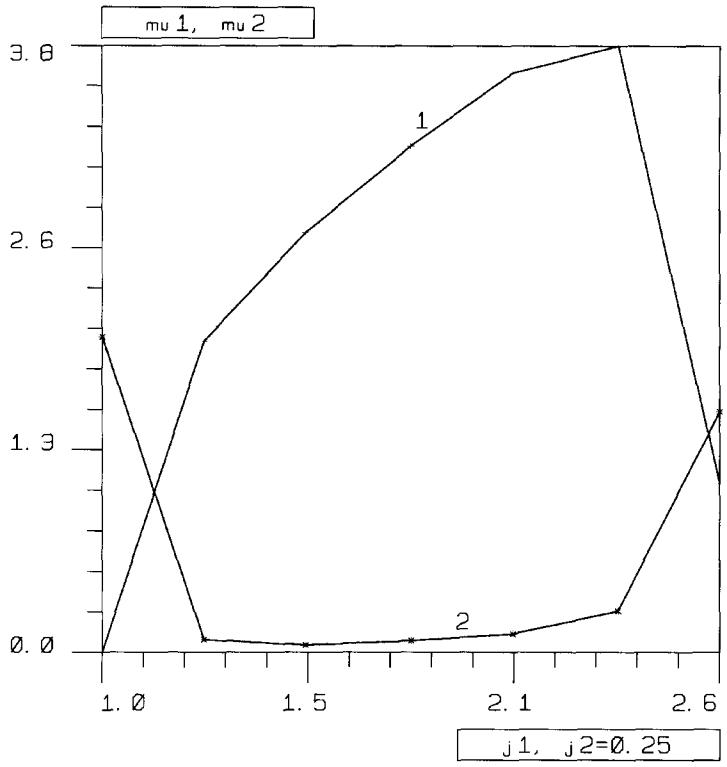

Fig. 2. Parameters μ_1 (1) and μ_2 (2), as functions of j_1, for $j_2 = 0.25$ computed as described in Section 5.1. Both behave smoothly.

takes about 90 seconds of CPU per iteration on a CRAY-YMP computer. Note that the larger is the quotient, the faster is the convergence of the conjugate gradient process.

Fig. 2 shows the computed μ_1 and μ_2 versus the invariant j_1, for $j_2 = 0.25$. A continuous behaviour, without too large gradients, is observed.

5.2. *Asymptotic behaviour of closure terms*

The technique of computation of closure terms that we have developed above allows to compute these terms in a relatively small region of $\widehat{D}$ around the identity. However, in practice the computing times for each actual values of j_1 and j_2 turn out to be very long, and so it is interesting to study the asymptotic behaviour of $\Phi(\widehat{D})$ in j_1 and j_2.

Let us give a fixed value to j_2, and assume that $\widetilde{w}_1$, $\widetilde{w}_2$ and $\widetilde{w}_3$ admit asymptotic expansions in terms of $\sigma = 1/\sqrt{j_1}$ as

$$\begin{cases} \widetilde{w}_1 = \widetilde{w}_1^{(0)} + \sigma\widetilde{w}_1^{(1)} + \mathrm{O}(\sigma^2), \\ \widetilde{w}_2 = \widetilde{w}_2^{(0)} + \sigma\widetilde{w}_2^{(1)} + \mathrm{O}(\sigma^2), \\ \widetilde{w}_3 = \widetilde{w}_3^{(0)} + \sigma\widetilde{w}_3^{(1)} + \mathrm{O}(\sigma^2). \end{cases} \tag{28}$$

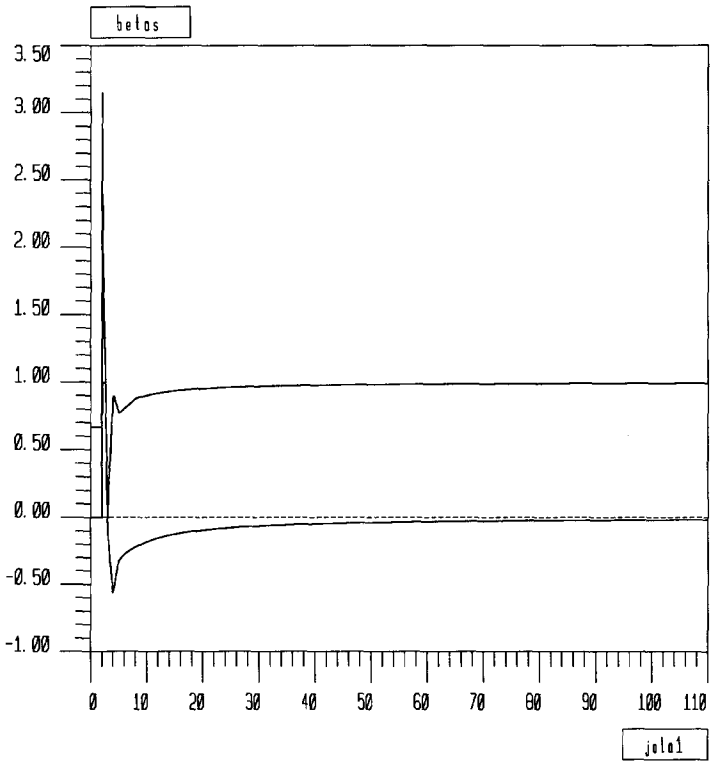

Fig. 3. Closure parameters β_0 and β_1 as functions of j_1, for $j_2 = 1$, corresponding to actual tabulations. High oscillations appear near the identity matrix.

According to [4], it is possible to give an initial condition for the microstructure problem (26) compatible with this expansion:

$$\widetilde{w}_0(y) = \sigma w_0'(y_2), \tag{29}$$

where w_0' has unit kinetic energy and depends only on y_2. Following now [12], we may conclude that the only expansions (28) compatible with the Euler equations appearing in (26) correspond to

$$\widetilde{w}_1^{(0)} = \widetilde{w}_2^{(0)} = \widetilde{w}_3^{(0)} = 0.$$

This yields $\widetilde{w} = \mathrm{O}(j_1^{-1/2})$ and so $\widetilde{R} = \mathrm{O}(j_1^{-1})$ as $j_1 \to \infty$.

The numerical solutions to problem (26) performed for diagonal matrices roughly follow this behaviour for large enough j_1 (see Tables 1, 2 and also Fig. 3).

Another possible asymptotic behaviour is obtained numerically if matrix C in (26) is taken with the following structure [3]:

$$C = \left[\begin{array}{cc|c} 1 & \alpha & \\ \alpha & 1+\alpha^2 & \\ \hline & & 1 \end{array}\right].$$

Table 1
Computed values of parameter c_1, such that $\mu_1 \simeq c_1(j_2)/j_1$ as $j_1 \to \infty$

$j_2 \backslash j_1$	3.00	4.00	5.00	8.00	20.00	102.00
0.9					2.16	3.02
1.0	0.21	0.74	2.07	2.22	2.39	2.39
1.1					2.62	3.19

Table 2
Computed values of parameter c_2, such that $\mu_2 \simeq c_2(j_2)/j_1$ as $j_1 \to \infty$

$j_2 \backslash j_1$	3.00	4.00	5.00	8.00	20.00	102.00
0.9					1.76	1.81
1.0	5.89	7.25	2.32	1.90	1.95	2.02
1.1					2.14	2.20

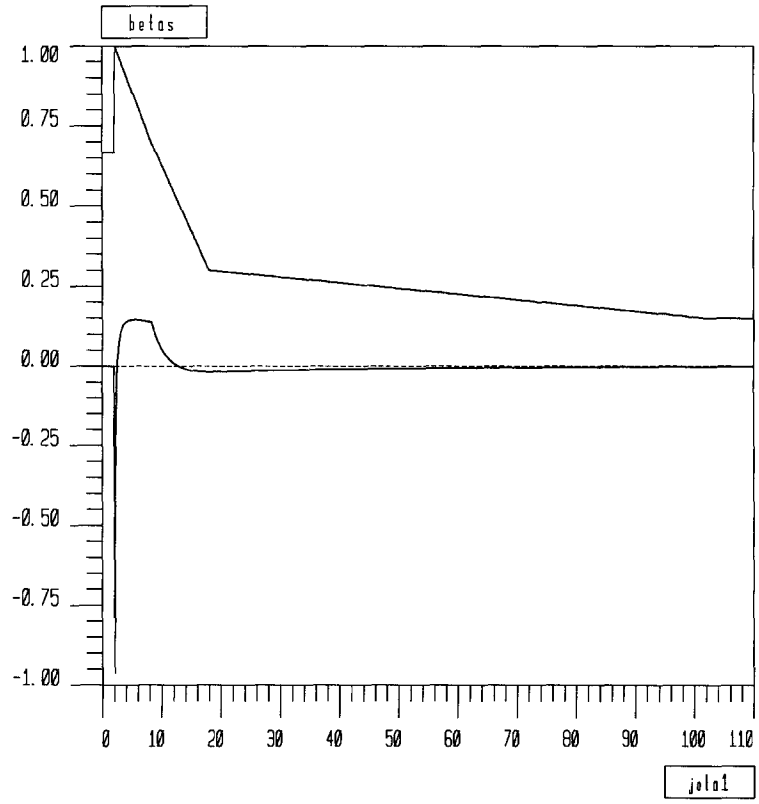

Fig. 4. Closure parameters β_0 and β_1 as functions of j_1, for $j_2 = 1$. The oscillations near the identity matrix are less pronounced.

Notice that in this case is $j_2 = 1$, $\forall \alpha$. The tabulations performed in [3] show that parameters μ_1 and μ_2 tend to constant values as $j_2 \to \infty$ (see Fig. 4).

6. Change of variables

We shall adapt the numerical method introduced by Le Ribault in [8] to the solution of our model for 2D flows. This is a mixed finite element–finite volume method based upon a laminar version proposed by Rostand [14]. In particular, it needs a reformulation of the model equations in order to have the same law of state as in the laminar case (law of perfect gases). This allows to solve our model equations with any numerical technique developed for 2D Euler equations if the "physical" variables (density, velocity and energy) are decoupled from the "turbulent" ones (k and ε). In particular, Rostand's solver, that uses Roe's scheme for 1D flows across cell boundaries.

This reformulation is made up via the following change of variables:

$$q = p + \beta_0 \rho k, \qquad E' = E + \beta \rho k, \quad \text{with } \beta = -1 + \beta_0/(\gamma - 1). \tag{30}$$

Then, E' and q are indeed related by the law of perfect gases:

$$q = (\gamma - 1)\left(E' - \tfrac{1}{2}\rho |u|^2\right).$$

The equation for E' is obtained from that for E:

$$\frac{\partial E'}{\partial t} + \nabla \cdot \left[(E' + q)u\right]$$

$$= \left\{ \frac{\partial E}{\partial t} + \nabla \cdot \left[(E + q)u\right] \right\} + \beta \left\{ \frac{\partial (\rho k)}{\partial t} + \nabla \cdot (\rho k u) \right\} + k \left\{ \frac{\partial (\rho \beta)}{\partial t} + \nabla \cdot (\rho \beta u) \right\}.$$

The first and second terms in the right-hand side here are respectively given by equations for E and k in system (12). To obtain the third one, observe that

$$\begin{cases} \dfrac{\partial j_1}{\partial t} + u \nabla j_1 = -2\widehat{D} : \nabla u, \\ \dfrac{\partial j_2}{\partial t} + u \nabla j_2 = -2 j_2 \nabla \cdot u. \end{cases} \tag{31}$$

This yields

$$\frac{\partial (\rho \beta)}{\partial t} + \nabla \cdot (\rho \beta u) = -\frac{2\rho}{\gamma - 1} \left(\widehat{D} : \nabla u \frac{\partial \beta_0}{\partial j_1} + j_2 \nabla \cdot u \frac{\partial \beta_0}{\partial j_2} \right).$$

This leads to the definitive 2D formulation of our model. In conservative form, this is

$$\frac{\partial}{\partial t} W + \nabla \cdot F(W) = \frac{1}{\mathrm{Re}} \nabla \cdot R(W, \nabla W) + \frac{1}{\mathrm{Re_T}} \nabla \cdot \overline{R}(W, \nabla W) + S(W), \tag{32}$$

with

$$W = \begin{bmatrix} \rho \\ \rho u_1 \\ \rho u_2 \\ E' \\ \rho k \\ \rho \varepsilon \\ \rho a_1 \\ \rho a_2 \end{bmatrix}, \qquad F_1(W) = \begin{bmatrix} \rho u_1 \\ \rho u_1 u_1 + q \\ \rho u_1 u_2 \\ (E' + q)u_1 \\ \rho k u_1 \\ \rho \varepsilon u_1 \\ \rho a_1 u_1 \\ \rho a_2 u_1 \end{bmatrix}, \qquad F_2(W) = \begin{bmatrix} \rho u_2 \\ \rho u_1 u_2 \\ \rho u_2 u_2 + q \\ (E' + q)u_2 \\ \rho k u_2 \\ \rho \varepsilon u_2 \\ \rho a_1 u_2 \\ \rho a_2 u_2 \end{bmatrix};$$

$R = (R_1, R_2)$, with

$$R_1(W, \nabla W) = \begin{bmatrix} 0 \\ \mathcal{T}_{xx} \\ \mathcal{T}_{xy} \\ \mathcal{T}_{xx} u_1 + \mathcal{T}_{xy} u_2 + \dfrac{\gamma}{\mathrm{Pr}} \dfrac{\partial e}{\partial x} \\ \dfrac{\partial k}{\partial x} \\ \dfrac{\partial \varepsilon}{\partial x} \\ 0 \\ 0 \end{bmatrix}, \qquad R_2(W, \nabla W) = \begin{bmatrix} 0 \\ \mathcal{T}_{xy} \\ \mathcal{T}_{yy} \\ \mathcal{T}_{xy} u_1 + \mathcal{T}_{yy} u_2 + \dfrac{\gamma}{\mathrm{Pr}} \dfrac{\partial e}{\partial y} \\ \dfrac{\partial k}{\partial y} \\ \dfrac{\partial \varepsilon}{\partial y} \\ 0 \\ 0 \end{bmatrix};$$

$\mathcal{T}_{xx}$, $\mathcal{T}_{xy}$, $\mathcal{T}_{yy}$ are the components of the viscous stress tensor, namely

$$\mathcal{T}_{xx} = \frac{2}{3}\mu\left(2\frac{\partial u_1}{\partial x} - \frac{\partial u_2}{\partial y}\right), \qquad \mathcal{T}_{xy} = \mu\left(\frac{\partial u_1}{\partial x} + \frac{\partial u_2}{\partial y}\right), \qquad \mathcal{T}_{yy} = \frac{2}{3}\mu\left(2\frac{\partial u_2}{\partial y} - \frac{\partial u_1}{\partial x}\right);$$

$\overline{R} = (\overline{R}_1, \overline{R}_2)$, with

$$\overline{R}_1(W, \nabla W) = \begin{bmatrix} 0 \\ \mathcal{T}_{xx} - \widehat{\beta}_1 \rho k \widehat{B}_{11} \\ \mathcal{T}_{xy} - \widehat{\beta}_1 \rho k \widehat{B}_{12} \\ (\mathcal{T}_{xx} - \widehat{\beta}_1 \rho k \widehat{B}_{11}) u_1 + (\mathcal{T}_{xy} - \widehat{\beta}_1 \rho k \widehat{B}_{12}) u_2 + \dfrac{\gamma}{\mathrm{Pr_T}} \dfrac{\partial e}{\partial x} + \dfrac{1}{\sigma_k} \dfrac{\partial k}{\partial x} \\ \dfrac{1}{\sigma_k} \dfrac{\partial k}{\partial x} \\ \dfrac{1}{\sigma_\varepsilon} \dfrac{\partial \varepsilon}{\partial x} \\ 0 \\ 0 \end{bmatrix},$$

$$\overline{R}_2(W, \nabla W) = \begin{bmatrix} 0 \\ \mathcal{T}_{xy} - \widehat{\beta}_1 \rho k \widehat{B}_{12} \\ \mathcal{T}_{yy} - \widehat{\beta}_1 \rho k \widehat{B}_{22} \\ (\mathcal{T}_{xy} - \widehat{\beta}_1 \rho k \widehat{B}_{12}) u_1 + (\mathcal{T}_{yy} - \widehat{\beta}_1 \rho k \widehat{B}_{22}) u_2 + \dfrac{\gamma}{\mathrm{Pr_T}} \dfrac{\partial e}{\partial y} + \dfrac{1}{\sigma_k} \dfrac{\partial k}{\partial y} \\ \dfrac{1}{\sigma_k} \dfrac{\partial k}{\partial y} \\ \dfrac{1}{\sigma_\varepsilon} \dfrac{\partial \varepsilon}{\partial y} \\ 0 \\ 0 \end{bmatrix},$$

where $\widehat{\beta}_1 = \beta_1 \mathrm{Re_T}$;

$$S(W) = \begin{bmatrix} 0 \\ 0 \\ 0 \\ \psi_k \\ -P + \rho\varepsilon \\ C_{\varepsilon 1} \dfrac{\varepsilon}{k} P - C_{\varepsilon 2} \rho \dfrac{\varepsilon^2}{k} \\ 0 \\ 0 \end{bmatrix};$$

and finally

$$\psi_k = \beta\left(\frac{\partial(\rho k)}{\partial t} + \nabla\cdot(\rho k u)\right) - \frac{2}{\gamma-1}\rho k\left(\widehat{D}:\nabla u\frac{\partial\beta_0}{\partial j_1} + j_2\nabla\cdot u\frac{\partial\beta_0}{\partial j_2}\right).$$

Notice that in (32), as usual,

- the term $(\partial/\partial t)W + \nabla\cdot F(W)$ represents the convective flux,
- the term $(1/\mathrm{Re})\nabla\cdot R(W,\nabla W)$ represents the molecular diffusion,
- the term $(1/\mathrm{Re_T})\nabla\cdot \overline{R}(W,\nabla W)$ represents the turbulent diffusion, and
- the term $S(W)$ represents the turbulent production.

7. Numerical discretization

In this section we shall describe the main issues concerning the adaptation of Le Ribault's solver [8] to the numerical solution of model (32).

7.1. A mixed finite element–finite volume space discretization

The space discretization is an adaptation of that introduced in [14] for laminar flows, and adapted in [8] to the k–ε model.

Let us consider a triangulation $\mathcal{T}_h$ of the (polygonal) computational domain Ω. For each node α_i of $\mathcal{T}_h$, call C_i the finite volume cell associate to α_i. The sides of this cell are the medians of sides of the triangles of $\mathcal{T}_h$, one of whose vertex is α_i.

Let us define the space of piecewise constant functions

$$Z_h = \{z_h : \Omega \mapsto \mathbb{R} \mid z_h|_{C_i} \text{ is constant, } \forall i \text{ node of } \mathcal{T}_h\},$$

and the space of continuous piecewise affine functions

$$Y_h = \left\{y_h \in C^0(\overline{\Omega}) \mid y_h|_T \text{ is affine, } \forall T \in \mathcal{T}_h\right\}.$$

Define the transformation

$$\varsigma_h : Y_h \mapsto Z_h$$

by

$$\varsigma_h(y_h)|_{C_i} = y_h(\alpha_i), \quad \forall \alpha_i \text{ node of } \mathcal{T}_h.$$

Then ς_h is bijective. We shall consider both the approximation y_h and $\varsigma_h(y_h)$ of a given function defined in Ω.

Our variational discretization of (32) is the following:

$$\begin{cases} \text{To find } W_h \in Y_h^8 \text{ such that} \\ \displaystyle\int_\Omega \frac{\partial W_h}{\partial t}\varsigma_h(\phi_h)\,\mathrm{d}x + \int_\Omega \nabla\cdot\big[F(W_h)\big]\varsigma_h(\phi_h)\,\mathrm{d}x \\ \quad = \dfrac{1}{\mathrm{Re}}\displaystyle\int_\Omega \nabla\cdot R(W_h,\nabla W_h)\phi_h\,\mathrm{d}x + \frac{1}{\mathrm{Re}_T}\int_\Omega \nabla\cdot \overline{R}(W_h,\nabla W_h)\phi_h\,\mathrm{d}x \\ \quad + \displaystyle\int_\Omega S(W_h)\phi_h\,\mathrm{d}x, \quad \forall \phi_h \in Y_h^8. \end{cases} \tag{33}$$

In order to perform a practical calculation of (33), we follow all steps given in [8]: the convective fluxes are computed by Van Leer's MUSCL (Monotonic Upstream Schemes for Conservation Laws) second-order method [17]. The diffusive terms are computed after integration by parts. For instance,

$$\int_\Omega \nabla\cdot\overline{R}(W_h,\nabla W_h)\phi_h\,\mathrm{d}x = \int_{\partial\Omega} \overline{R}(W_h,\nabla W_h)\cdot n\phi_h\,\mathrm{d}x - \int_\Omega \left(\overline{R}_1\frac{\partial\phi_h}{\partial x_1} + \overline{R}_2\frac{\partial\phi_h}{\partial x_2}\right)\mathrm{d}x.$$

The contribution of the boundary integral is neglected (it is assumed that its contribution for large Reynolds number is irrelevant). To approximate the remaining integral, W_h is discretized by a triangle-by-triangle constant value $\widetilde{W}_h$. This value is calculated by averaging W_h on each triangle. Then

$$\begin{aligned} &\int_\Omega \left(\overline{R}_1\frac{\partial\phi_h}{\partial x_1} + \overline{R}_2\frac{\partial\phi_h}{\partial x_2}\right)\mathrm{d}x \\ &\quad \simeq \sum_{T\in\mathcal{T}_h}\left[\overline{R}_1\big(\widetilde{W}_h|_T,\nabla W_h|_T\big)\frac{\partial\phi_h|_T}{\partial x_1} + \overline{R}_2\big(\widetilde{W}_h|_T,\nabla W_h|_T\big)\frac{\partial\phi_h|_T}{\partial x_2}\right]|T|. \end{aligned}$$

In our case, this requires to know a constant value for $\widehat{D}$ and β_1 on each triangle of $\mathcal{T}_h$.

Finally, the computation of the source term in (33) is again performed by approximating $S(W_h)$ by the piecewise constant function $S(\widetilde{W}_h)$. Note that this requires to know a constant value of β, $\partial\beta_0/\partial j_1$ and $\partial\beta_0/\partial j_2$ on each triangle of $\mathcal{T}_h$.

The computation of new closure terms due to homogenization requires the computation of the inverse Lagrangian coordinates associated to the mean velocity field.

To do this, Eq. (4) has been rewritten as

$$\frac{\partial b}{\partial t} + \nabla\cdot(u\otimes b) = 0, \tag{34}$$

where $b = \rho a$.

To solve Eq. (34) we have adapted the finite volume technique of [8]. We just need to compute the flow between neighbouring cells by means of Van Leer's MUSCL method. This, together with a

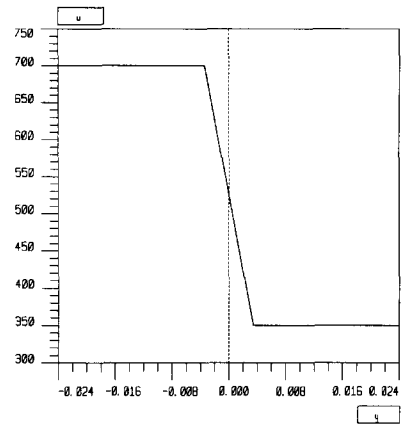

(a)

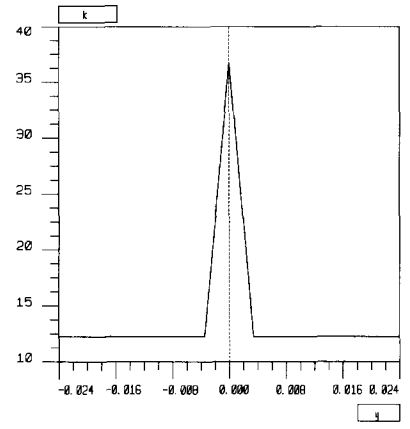

(b)

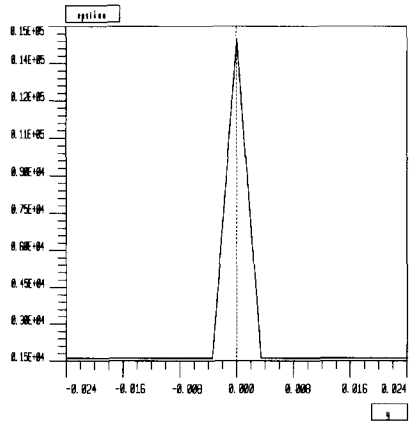

(c)

Fig. 5. Initial profiles for: (a) velocity u, (b) kinetic energy k, and (c) turbulent dissipation ε. The values represented correspond to the initial conditions for $M_c = 0.1$. For larger values of M_c the velocity has been rescaled.

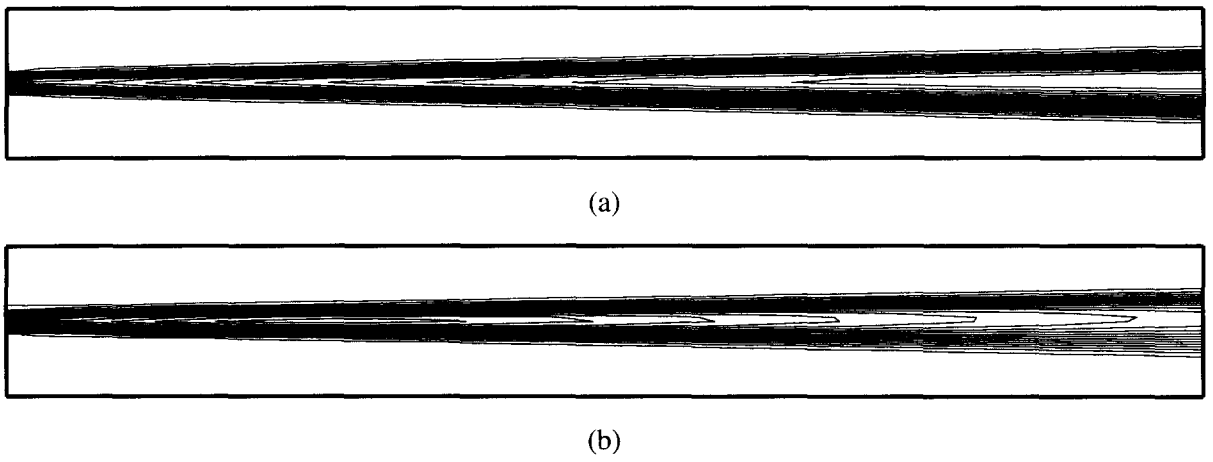

(a)

(b)

Fig. 6. Isolines of (a) k and (b) ε for $M_c = 0.45$. Computed with a grid of 2180 nodes.

first order accuracy in time, yields a remarkable increase of accuracy. To test this technique, we have solved Eq. (34) with a given velocity field, that presents a large shear in a small interval:

$$u_1 = \big(u_1(x_2), 0\big)^*, \quad \text{with } u_1(x_2) = \begin{cases} 1, & \text{if } 0.01 \leqslant x_2 \leqslant 1, \\ 1 - 50(x - 0.01), & \text{if } -0.01 \leqslant x_2 \leqslant 0.01, \\ 2, & \text{if } -1 \leqslant x_2 \leqslant -0.01. \end{cases}$$

Fig. 6 represents the isolines of the computed a_h at time $t = 1$. A good resolution is attempted.

Notice that if ∇a_h is nonsingular, the (j_1, j_2) values computed by our numerical scheme always lie in the admissible region. Indeed, we compute a constant value G_T of ∇a_h on each triangle T. Then, $C_T = G_T^* G_T$ is always positive semidefinite. If in addition ∇a_h is nonsingular, then C_T is positive definite.

7.2. Boundary conditions

Boundary conditions are imposed in a weak sense after integration by parts in (33): Assume ϕ_h is a base function of Y_h located at node $\alpha_i \in \Gamma = \partial\Omega$. Then

$$\Gamma_i = \Gamma \cap \partial C_i \neq \emptyset.$$

The imposed boundary conditions are as follows:

$$\int_{\Gamma_i} F(W_h) \cdot n \, \mathrm{d}\Gamma - \frac{1}{\mathrm{Re}} \int_{\Gamma \cap \mathrm{Sop}(\phi_h)} R(W_h, \nabla W_h) \cdot n \, \phi_h \, \mathrm{d}\Gamma$$
$$- \frac{1}{\mathrm{Re_T}} \int_{\Gamma \cap \mathrm{Sop}(\phi_h)} \overline{R}(W_h, \nabla W_h) \cdot n \, \phi_h \, \mathrm{d}\Gamma = \int_{\Gamma_i} \overline{F}(W_h, W_\infty, n) \, \mathrm{d}\Gamma. \tag{35}$$

Here, $\overline{F}$ is a suitable flux function on Γ, and W_∞ represents the data. Depending on the actual structure of $\overline{F}$ we shall impose a specific kind of boundary conditions on each particular variable.

For instance, for the physical variables $(\rho, \rho u_1, \rho u_2, E')^*$, $\overline{F}$ is given by means of a Steger–Warming flux [16]: The flux function F for those variables verifies

$$F(W) \cdot n = A(W, n)W,$$

where

$$A(W, n) = \frac{\partial F_1}{\partial W} n_1 + \frac{\partial F_2}{\partial W} n_2.$$

Let us recall that $A(W, n)$ is diagonalizable as $A(W, n) = P(W, n)\Lambda P^{-1}(W, n)$ with

$$\Lambda = \operatorname{diag}(\lambda_1, \lambda_2, \lambda_3, \lambda_4), \quad \begin{cases} \lambda_1 = \lambda_2 = u \cdot n, \\ \lambda_3 = u \cdot n + c, \\ \lambda_4 = u \cdot n - c. \end{cases}$$

The Steger–Warming flux on the boundary Γ may be written by

$$\overline{F}(W, W_\infty, n) = A^+(W, n)W + A^-(W, n)W_\infty.$$

The actual choice of W_∞ depends on whether we are considering inlet or outlet boundaries. The actual structure of the Steger–Warming flux acts as a kind of filter that selects the appropriate number of Dirichlet boundary conditions, depending on whether the flow is sub or supersonic. For inlet boundary, we take

$$W_\infty = \left(\rho_\infty, \rho_\infty u_{1\infty}, \rho_\infty u_{2\infty}, E'_\infty\right)^*.$$

For outlet boundary, we take

$$W_\infty = \left(\rho, \rho u_1, \rho u_2, E'_\infty\right)^*, \quad \text{where } E'_\infty = \frac{q_\infty}{\gamma - 1} + \tfrac{1}{2}\rho|u|^2.$$

In this way, we may impose the pressure on the outlet flow boundary when the flow is subsonic.

Also, we may impose free-slip boundary conditions in the part of Γ where the normal flow $u \cdot n$ is zero. In this case, we define $\overline{F}(W, W_\infty, n) = (0, 0, 0, pn_1, pn_2, 0, 0, 0)^*$. In particular, this yields

$$\frac{\partial k}{\partial n} = 0, \qquad \frac{\partial \varepsilon}{\partial n} = 0, \qquad \frac{\partial e}{\partial n} = 0.$$

In the case of the other variables, a_1, a_2, k and ε, the definition of the boundary flow $\overline{F}$ is simpler. In the inlet flow boundary, we define

$$\overline{F}(W, W_\infty, n) = F(W_\infty) \cdot n.$$

In particular, k_∞ and ε_∞ must be provided. Also, $a_\infty = x - u_\infty t$. In the outlet boundary, we define

$$\overline{F}(W, W_\infty, n) = F(W) \cdot n.$$

It is interesting to observe that in condensated form we are imposing the following boundary conditions:

$$\left[F(W) - \frac{1}{\mathrm{Re}} R(W, \nabla W) - \frac{1}{\mathrm{Re_T}} \overline{R}(W, \nabla W)\right] \cdot n = \overline{F}(W, W_\infty, n). \tag{36}$$

Then, we do not impose "true" inlet Dirichlet boundary conditions, as we are neglecting the diffusion term in our integration by parts. However, for turbulent flows, the diffusion coefficients will become very small and inlet boundary conditions will be predominantly of Dirichlet kind.

7.3. Time discretization

We have adapted the second-order four-step explicit Runge–Kutta scheme used in [8]. To solve the Cauchy problem

$$\begin{cases} y'(t) = f\big(t, y(t)\big) & \text{in } [t_0, t_0 + T], \\ y(t_0) = y_0, \end{cases}$$

this scheme updates y_n to y_{n+1} in four intermediate steps:

$$\begin{cases} y_{n,0} = y_n, \qquad t_{n,0} = t_n, \\ y_{n,k} = y_n + \alpha_k \Delta t^n f(t_{n,k-1}, y_{n,k-1}), \quad t_{n,k} = t_n + \alpha_k \Delta t^n, \quad k = 1,2,3,4, \\ y_{n+1} = y_{n,4}, \qquad t_{n+1} = t_{n,4}, \end{cases} \tag{37}$$

where $t_0 = 0$, $y_0 = y(t_0)$, $\alpha_1 = 0.11$, $\alpha_2 = 0.2766$, $\alpha_3 = 0.5$ and $\alpha_4 = 1.0$.

This scheme requires as low memory requirements as the Euler method, although it is second-order accurate and bears much better stability properties.

In our case we use this scheme, but we split our variables into three blocks:

$$W^{(1)} = \begin{bmatrix} \rho \\ \rho u_1 \\ \rho u_2 \\ E' \end{bmatrix}, \qquad W^{(2)} = \begin{bmatrix} \rho k \\ \rho \varepsilon \end{bmatrix}, \qquad W^{(3)} = \begin{bmatrix} \rho a_1 \\ \rho a_2 \end{bmatrix} = \rho a.$$

Our time-stepping strategy has been the following:

Given $W_{n,0} = W_n$, compute recursively $W_{n,k}$ for $k = 1,2,3,4$ by

1. Update $W^{(3)}_{n,k}$ to $W^{(3)}_{n,k+1}$ by (37), and then compute $a_{n,k+1}$;
2. Compute all closure terms from $a_{n,k+1}$;
3. Update $W^{(1)}_{n,k}$ to $W^{(1)}_{n,k+1}$ by (37);
4. Update $W^{(2)}_{n,k}$ to $W^{(2)}_{n,k+1}$ by (37).

Set $W_{n+1} = W_{n,4}$.

Note that the conservative variables in $W^{(1)} = (\rho, \rho u_1, \rho u_2, E')^*$ satisfy the perfect gas state law, and that the convection operator acting on $W^{(1)}$ is the same as for 2D Euler equations. Thus, any flux-splitting technique that is well suited for 2D Euler equations may be used to update $W^{(1)}_n$ in the above time-stepping strategy. In our case, we have used Roe's scheme. This yields a numerical scheme with a first-order overall accuracy. The "k–ε model" variables are computed with second-order accuracy in space, and the "homogenization" variables and new closure terms are only first-order accurate. At

first, it does not seem necessary to compute closure terms with second-order accuracy, as the tabulated closure terms remain only temptative.

8. Numerical tests

We have performed some initial numerical tests of our numerical code for steady sub- and supersonic mixing layers. Low Mach mixing layers is a good test case, as accurate experimental measurements are available [1]. Moreover, the results furnished by the k–ε model are well known, and reasonably accurate with respect to experimental measurements [7]. Thus, it is a good test to analyze the consistency of our model with the k–ε one for steady flows. As our model essentially takes into account purely transient effects, no large differences with the k–ε model should be expected for steady flows.

Also, for intermediate and high Mach mixing layers, k–ε models yield more inaccurate results as it does not take into account some relevant effects of the compressibility of the small scales. However, this is a good test case to observe the numerical performances (stability, verification of boundary conditions, convergence to a steady state, grid independence) of our code.

For compressible mixing layer, the relevant similarity parameter to define the flow is the convective Mach number M_c. Denote respectively by M_1 and M_2 the Mach numbers and by a_1 and a_2 the sound speeds in the upper and lower layers. The convective Mach number is defined as

$$M_c = \frac{M_2 - M_1}{a_1 + a_2},$$

when $M_2 > M_1$. In our computations, we have taken the same gas at both sides of the layer, i.e., $a_1 = a_2$.

We have carried out numerical tests for convective Mach numbers of $M_c = 0.45$, $M_c = 0.65$ and $M_c = 1$ which correspond to initial and inlet Mach numbers of $M_1 = 1.37$, $M_1 = 1.98$ and $M_1 = 3.04$, and of $M_2 = 1.89$, $M_2 = 2.74$ and $M_2 = 4.23$, respectively.

We have considered the profiles for dimensionless initial conditions for u, k and ε given in Fig. 5. Also, our reference magnitudes have been $L_0 = 48$ mm, $u_0 = 700$ m/s, $\rho_0 = 0.295$ kg/m^3, $T_0 = 334.4^0$K, $p_0 = 28302.4$ Pa, $\mu_0 = 1.147 \times 10^{-5}$. The velocity profiles have been rescaled to change the convective Mach number. This is a test case precedingly used by Guezengar et al. in [7] to test the k–ε model.

As computational domain we have taken a square box with sides of lengths 50 and 400 mm. Free slip boundary conditions have been imposed on the (artificial) upper and lower boundaries. Also, inflow boundary conditions are those given by the restriction of the initial conditions to the inflow boundary. Finally, homogeneous Neumann boundary conditions are imposed in the outflow boundary on all variables, except for the pressure if flow is subsonic, which is imposed in this case.

For M_c up to 0.45, this flow reaches a steady state which is attained by the k–ε model, even for coarse grids. Our model also reaches a steady state with a coarse grid of 290 nodes. For larger M_c, standard k–ε model reaches an almost steady state, with typical residuals of order 10^{-3} that oscillate slightly [7]. We have found a similar behaviour for our code in these cases. In all tests considered, our results are quite grid-independent for grids of over 2000 nodes, approximately. Moreover, the code shows good stability properties for all cases considered, although the time steps are shorter for larger Mach numbers, as expected.

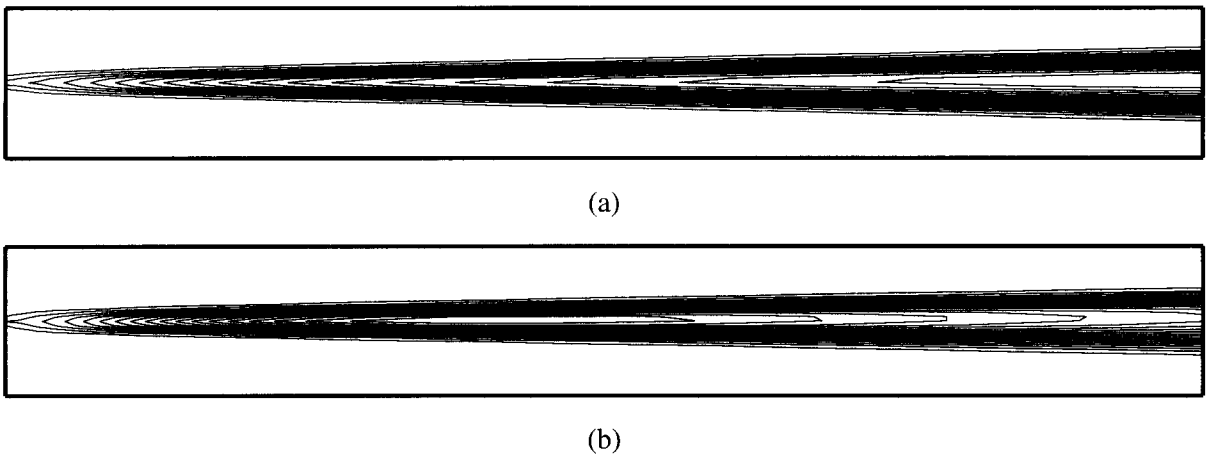

(a)

(b)

Fig. 7. Isolines of (a) k and (b) ε for $M_c = 1$. Computed with a grid of 2180 nodes. The overall values, and in particular the maximum, of k are larger for $M_c = 1$ than for $M_c = 0.45$.

To test the two possible sets of closure terms referenced in Section 4, we have performed an initial test with $M_c = 0.2$. If the first kind of closure terms, obtained by Chacón in [3] are used, the results are quite close to those given by the k–ε model. For instance, the steady states obtained for k are almost indistinguishable. Also, mean velocity profiles are almost exactly the same. This probably happens because for these closure terms, the additional term $\beta_1 \widehat{B}$ introduced in the RST is small, for both small or large values of j_1. Thus, for these closure terms our numerical results are consistent with the fact that we are essentially modelling unsteady turbulence.

If the other kind of closure terms referenced in Section 4 are used, the code turns to be somehow unstable and some unphysical features appear in the results obtained. In particular, the accuracy of the computed expansion rate of the layer decreases largely as the longitudinal distance to the inflow boundary increases. Also, the free-slip boundary condition $u \cdot n = 0$ is not well satisfied in the low-velocity side of the layer. These unphysical results are very likely due to inaccuracies in the computation of the closure terms, that produce large oscillations of the closure functions β_0 and β_1. However, improving this accuracy would require a too large amount of computational work to solve the equation of the microstructures.

Thus, we have performed more extensive test using Chacón's closure terms, for convective Mach numbers of $M_c = 0.45$, $M_c = 0.65$ and $M_c = 1$. We compute smooth k and ε in all cases (see Fig. 6 for $M_c = 0.45$, and Fig. 7 for $M_c = 1$).

Self-similarity is a good test for this flow to analyze whether a numerical steady solution is physically acceptable [1]. The basic parameter to define self-similarity profiles of mixing layers is the thickness δ of the layer. Let us recall the Stanford Conference definition of δ [1]: denote by x the longitudinal variable along the layer, and by y the cross-flow variable. For each x, we define y_1 and y_2 such that

$$u(y_1) = u_1 + \sqrt{0.9}(u_2 - u_1),$$
$$u(y_2) = u_1 + \sqrt{0.1}(u_2 - u_1),$$

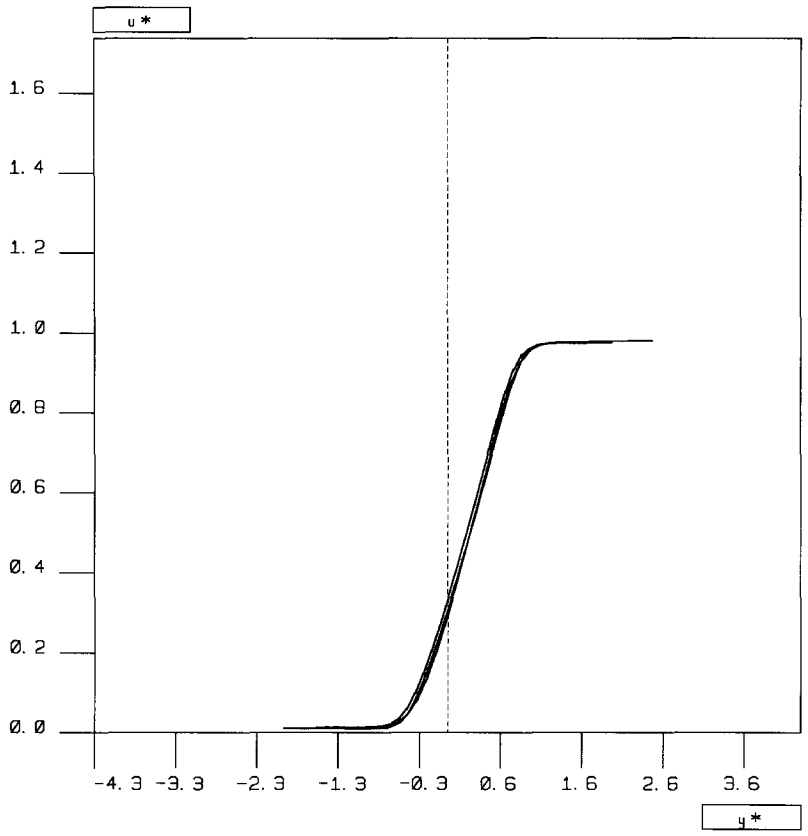

Fig. 8. Similarity profiles for the velocity at different distances from the leading edge: $x = 192$ mm, 288 mm and 384 mm. A good self-similarity is obtained.

where $u_1 < u_2$ are the two constant velocities on the sides of the layer. We then define the thickness as $\delta = |y_2 - y_1|$.

Now, we may define similarity profiles u^S and k^S for velocity and energy (for instance), as

$$u^S(x, y^S) = \frac{u(x,y) - u_1}{u_2 - u_1}, \quad k^S(x, y^S) = \frac{k(x,y)}{\max_y k(x,y)}, \quad \text{where } y^S = \frac{y}{\delta}.$$

We say that a solution is self-similar if the corresponding similarity profiles are independent of x. As we may observe in Figs. 8 and 9, our results yield good self-similar profiles for mean velocity and kinetic energy.

We also obtain a linear expansion of the thickness δ of the layer, as expected from experimental measurements (see Fig. 10). The spreading rate δ' in both cases takes a value close to the one corresponding to low convective Mach number δ'_0. The normalized spreading rate is in both cases $\delta'/\delta'_0 = 1.032$. In the case of standard k–ε model, this value is of 0.99 in both cases [7]. Thus, our results are close to those of standard k–ε, as expected. It should be remarked that these values do not agree with experimental results. Indeed, compressibility effects make the normalized spreading rate decay for $M_c \geqslant 0.45$, approximately, to a value which is kept constant for M_c between 1 and 4.

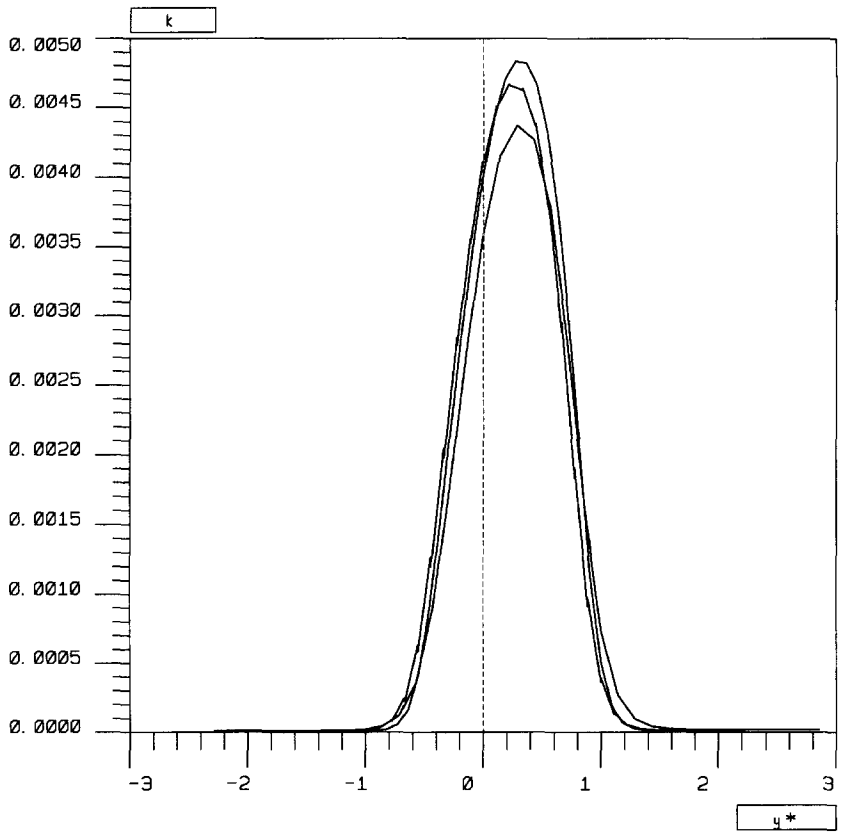

Fig. 9. Similarity profiles for the kinetic energy at different distances from the leading edge: $x = 192$ mm, 288 mm and 384 mm. Self-similarity is less strong than for the velocity, although it is still good.

Compressibility effects are taken into account in specific models such as Zeman's or Sarkar's [15,18]. These models introduce an increase of turbulence dissipation (ε) due to dilatation in the first one, and to solenoidal dissipation in the second one. However, these effects are not taken into account by the standard k–ε model. This is also the case of our model, as we are dealing only with perturbations which are incompressible with respect to the microscale variable.

9. Conclusions

In this work we have shown that the MPP averaging technique for flows with highly oscillating initial conditions introduced in [9] for incompressible flows may also be applied to perfect inviscid flows at moderate Mach numbers.

We have obtained a set of averaged equations where the closure terms are computed from the solution of a "microstructure" equations set that governs the small scale behaviour of the perturbation. In view of the experience acquired with incompressible flows, we have derived a k–ε type model in order to include eddy diffusion effects, and also the purely transient effects that are modelled by the

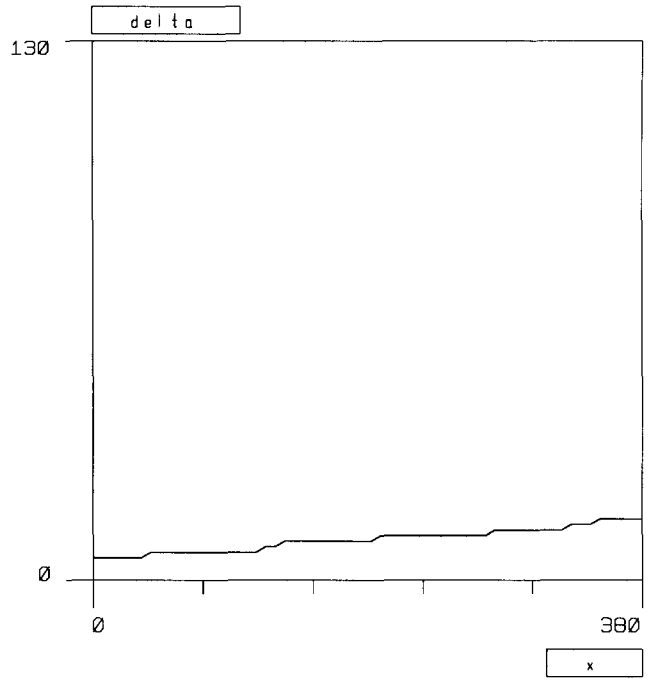

Fig. 10. Upper boundary of the mixing layer for $M_c = 0.45$. It presents an almost linear growth.

MPP averaging. We have obtained a 2D version of this model, for which the closure terms have a particularly simple structure. Moreover, we have adapted a technique of computation of these closure terms, based upon a least-squares formulation of the canonical microstructure problem.

Next, a mixed finite volume–finite element numerical solver for our 2D model has been derived. This solver is based upon a splitting of "physical", "turbulent" and auxiliary variables. Roe's scheme, combined with Van Leer's MUSCL second-order method are used to compute the numerical fluxes. This solver has been tested for steady mixing layer flow. The theoretical expectations of the model at moderate convective Mach numbers have been confirmed: the relevant mean quantities of this flow have been well predicted, much as the k–ε model.

We think that our results are encouraging, in the sense that they support the consistency of the model for steady flows. However, we are conscient of the fact that this testing is to be continued with purely transient flows, in order to analyze whether the model improves the predictions of current turbulence models, normally derived to model steady flows.

Acknowledgements

The authors wish to thank Dr. Dervieux (INRIA, Sophia-Antipolis) for his helpful disposition.

Some numerical experiments have been carried out on a CRAY YMP-EL machine at CIEMAT (Spain). We thank very much the attention that some CIEMAT researchers have granted us, especially Dr. J. Casado and Dr. M. Giménez.

References

[1] S. Barre, C. Quine and J.P. Dussauge, Compressibility effects on the structure of supersonic mixing layers: experimental results, *J. Fluid. Mech.* 259 (6) (1994) 47–78.
[2] C. Bègue, B. Cardot and O. Pironneau, Simulation of turbulence with transient mean, *Internat. J. Numer. Methods Fluids* 11 (1990) 677–695.
[3] T. Chacón, Oscillations due to the transport of microstructures, *SIAM J. Appl. Math.* 48 (5) (1988) 1128–1146.
[4] T. Chacón, D. Franco and F. Ortegón, Homogenization of incompressible flow with helical microstructures, *Adv. Math. Sci. Appl.* 1 (2) (1992) 251–300.
[5] T. Chacón and F. Ortegón, On a Rivlin–Eriksen's theorem application to a turbulence model, *European J. Mech. B Fluids* 14 (5) (1995).
[6] D. Franco, Ph.D. Thesis, University of Sevilla (in preparation).
[7] D. Guezengar and H. Guillard, Compressibility models applied to supersonic mixing layers, in: *Proceedings ETMA Meeting*, UMIST, Manchester (1994).
[8] C. Le Ribault, Simulation des écoulements turbulents compressibles par une méthode mixte éléments finis-volumes finis, Thèse de Doctorat, Université Lyon (1991).
[9] D. McLaughlin, G. Papanicolaou and O. Pironneau, Transport of microstructures and related problems, *SIAM J. Appl. Math.* 45 (5) (1985).
[10] B. Mohammadi and O. Pironneau, *Analysis of k–ε Turbulence Model* (Wiley-Masson, Paris, 1993).
[11] C. Olivier, Simulation numérique d'écoulements visqueux compressibles laminaires et turbulents, Thèse de Doctorat, Université Nice Sophia-Antipolis (1991).
[12] F. Ortegón, Modélisation des écoulements turbulents à deux échelles par méthode d'homogénéisation, Thèse de Doctorat, Université Paris VI (1989).
[13] W.C. Reynolds, Physical and analytical foundations concepts, and new directions in turbulence modeling and simulation, in: *Proceedings Ecole d'Eté CEA-EDF-INRIA d'Analyse Numérique et Modélisation Théorique de la Turbulence*, Clamart, France (1982).
[14] P. Rostand, Sur une méthode de volumes finis en maillage non structuré pour le calcul d'écoulements visqueux compressibles, Thèse de Doctorat, Université Paris VI (1989).
[15] S. Sarkar, Modelling the pressure–dilatation correlation, ICASE Report 91-42 (1991).
[16] J. Steger and R.F. Warming, Flux vector splitting for the inviscid gas dynamic with applications to finite difference methods, *J. Comput. Phys.* 40 (1981) 263–293.
[17] B. Van Leer, Flux vector splitting for the Euler equations, Lecture Notes in Physics 170 (1982) 405–512.
[18] O. Zeman, Dilatation dissipation: the concept and application in modelling compressible mixing layers, *Phys. Fluids* 2 (1990) 178–188.